

# The Kernel Two-Sample Test for Brain Networks

Emanuele Olivetti<sup>1,2</sup>, Sandro Vega-Pons<sup>1,2,3</sup>, and Paolo Avesani<sup>1,2</sup>

<sup>1</sup>NeuroInformatics Laboratory (NILab), Bruno Kessler  
Foundation, Trento, Italy

<sup>2</sup>Center for Mind and Brain Sciences (CIMeC), University of  
Trento, Italy.

<sup>2</sup>Pattern Analysis and Computer Vision (PAVIS), Istituto Italiano  
di Tecnologia, Genova, Italy.

November 20, 2015

## Abstract

In clinical and neuroscientific studies, systematic differences between two populations of brain networks are investigated in order to characterize mental diseases or processes. Those networks are usually represented as graphs built from neuroimaging data and studied by means of graph analysis methods. The typical machine learning approach to study these brain graphs creates a classifier and tests its ability to discriminate the two populations. In contrast to this approach, in this work we propose to directly test whether two populations of graphs are different or not, by using the kernel two-sample test (KTST), without creating the intermediate classifier. We claim that, in general, the two approaches provides similar results and that the KTST requires much less computation. Additionally, in the regime of low sample size, we claim that the KTST has lower frequency of Type II error than the classification approach. Besides providing algorithmic considerations to support these claims, we show strong evidence through experiments and one simulation.

## 1 Introduction

Recent work reported alterations on the structural and functional connectivity networks in patients with mental diseases like schizophrenia and Alzheimer [1, 2]. Moreover, in neuroimaging-based experiments, it has been shown that different mental states or stimuli can produce alterations on the functional connectivity networks [3, 4].

For these reasons, there is interest in analysis methods that study systematic differences between populations of networks, usually represented as graphs. A recent review of the methods available in the literature [5], describes three

main directions of research in this area: machine learning, statistical hypothesis testing and network science. In this work we focus on the machine learning approach and discuss its use within statistical hypothesis testing.

The use of machine learning on brain networks is a recent and promising approach with application in both clinical and cognitive neuroscience [6]. Generally, this approach consists of classifying graphs. Graphs are suitable data structures to represent brain networks, but they are difficult to be directly manipulated by machine learning algorithms. Therefore, graph classification commonly requires an intermediate step in which graphs are mapped into a feature space, where classifiers can be directly applied. Such mapping can be done either implicitly, by using graph kernels [7], or explicitly, by using the so called graph embedding techniques [8].

Different graph kernels have recently been used for the classification of neuroimaging data. In the brain decoding literature, we find applications of the shortest-path kernel [9], a custom-designed kernel based on pair-wise node connectivity [10] and the Weisfeiler-Lehman kernel [11, 12]. This last one has also been successfully applied to a mild cognitive impairment (MCI) study [13].

A popular approach to encode the network information into a graph is to define a common set of nodes for all graphs, e.g. anatomical regions of the brain. With this *one-to-one correspondence* between the nodes across the graphs, the information is stored in the corresponding weights of the edges, i.e. in the adjacency matrices. In such a setting, a simple graph embedding technique is obtained by unfolding the upper triangular part of the adjacency matrix into a vector. This approach has been used in [14] for a movie task experiment and in [4] for the classification of sleep stages. See Section 2.2 for a more detailed description of graph embeddings and graph kernels.

Classification algorithms, together with graph embeddings or kernels, are used to study systematic differences among different populations of brain graphs[5]. In such application, the classifier is trained on part of the data, in order to discriminate the two groups/conditions. Then, on the remaining part of the data, the classifier is used to quantify how it generalizes the discrimination to future unseen graphs. This is done by defining a performance measure, like classification accuracy, that, with respect of the phenomenon under investigation, is a measure of its *effect size*. Often, such measures are estimated with resampling procedures, e.g. cross-validation. Additionally, when using such measures as a test statistic, it is possible to study the significance of the phenomenon by means of a statistical procedure, e.g. the permutation test. Here, we call such test as *classification-based test* (CBT). The CBT is the core element of multiple scientific studies [15].

During the last decade, the machine learning community developed a novel way to combine kernel methods with statistical tests. Specifically, given two populations of objects and a kernel function to quantify the object's similarity, the *kernel two-sample test* (KTST) [16, 17] was proposed to conduct the hypothesis test whether two populations have the same distribution or not. The KTST is a non-parametric test based on the *maximum-mean discrepancy* (MMD) test statistic, a distance function for distributions that can be estimated

from data. The KTST operates a two-sample test between two sets of arbitrary objects and, differently from CBT, directly quantify the significance of the effect without creating an intermediate classifier.

In this work, we propose to use the KTST on brain graphs to directly test scientific hypotheses. To the best of our knowledge, the KTST has never been used in this context and the closest works in the literature are on neuroimaging data not involving graphs [18, 19].

We claim that, in the context of scientific/clinical experiments, the KTST is an alternative tool to the CBT and that, in general, provides comparable results.

We also claim that, in case of low sample size, the KTST may have higher sensitivity than CBT. This is motivated by the fact that the estimation process of MMD is simple and deterministic and does not require the definition of multiple parameters like CBT does. On the other hand, the test statistic in the CBT requires a more complex and non-deterministic estimation process, which introduces additional variability in the result. This occurs because of the competing need of fitting additional parameters within the classification algorithm, e.g. the regularization term of support vector machines (SVMs), and of the non-deterministic process of estimation, i.e. the random train/test split, especially in the case of resampling/cross-validation.

In this paper, as support to our claims, we present experiments on 14 neuroimaging datasets of graphs, covering different scientific questions from cognitive studies to clinical investigation, with and without the node correspondence property. Moreover, we adopt two graph embeddings and two graph kernels, to show the generality of our findings. Additionally, we present a simulation study, where we show graph classification in a simplified setting. With such simulation we study the probability of Type I and Type II error of KTST and CBT in case of low sample size. The results of the simulation show the advantage of KTST over CBT, in terms of lower frequency of Type II error and equivalent Type I error, and corroborate our findings on neuroimaging data.

The paper is structured as follows: in Section 2 we introduce the notation, we formally describe graph embeddings and kernels and we define the CBT and the KTST. In Section 3, we describe the datasets used in the experiments. In Section 4, we provide all the details and results of the experiments described above and of the simulation study. In Section 5 and Section 6, we discuss the results and conclude this work mentioning current limitations and future perspective.

## 2 Methods

In this section we introduce the notation, some basic concepts and proceed to explain graphs embeddings, graph kernels and hypothesis testing. With these ingredients we then formally present the classification-based test (CBT) and the proposed kernel two-sample test (KTST).

## 2.1 Notation and Basic Concepts

Let  $G = (V, E, \ell, \omega)$  be a graph, where  $V$  is the set of nodes,  $E \subset V \times V$  is the set of edges,  $\ell : V \rightarrow \Sigma$  is a function that assigns a label from an alphabet  $\Sigma$  to each node and  $\omega : E \rightarrow \mathbb{R}$  is a function that assigns a real weight value to each edge in the graph. In this work, the graph  $G$  represents the network data of the brain, e.g. resting state connectivity. Let  $\mathcal{G}$  be the space of all simple, undirected, node-labeled and edge-weighted graphs, i.e.  $G \in \mathcal{G}$ .

Let  $Y \in \mathcal{Y}$  be a categorical random variable indicating the population/category of a graph  $G$ . Here we assume that  $Y$  is binary, e.g.  $\mathcal{Y} = \{\text{healthy}, \text{disease}\}$ , and for notational convenience we indicate  $\mathcal{Y} = \{a, b\}$  from now on.

A neuroimaging experiment over  $N$  subjects produces a dataset  $D = \{(g_1, y_1), \dots, (g_N, y_N)\}$  of  $N$  graphs drawn i.i.d. from an unknown probability distribution  $P_{\mathcal{G} \times \mathcal{Y}}$ . In a typical neuroimaging study,  $N$  is in the range 10 – 200.

In the terminology of two-sample tests, the two samples within  $D$  are  $A = \{g : (g, y) \in D, y = a\}$  and  $B = \{g : (g, y) \in D, y = b\}$ , where  $m = |A|$ ,  $n = |B|$ , such that  $N = m + n$ . From this point of view,  $A$  is sampled from  $P_{\mathcal{G}|y=a}$  and  $B$  from  $P_{\mathcal{G}|y=b}$ . In the following, for notational convenience, we call  $P_{\mathcal{G}|y=a}$  and  $P_{\mathcal{G}|y=b}$  as  $P_A$  and  $P_B$ .

## 2.2 Graphs: Kernels and Embeddings

A graph kernel  $k : \mathcal{G} \times \mathcal{G} \rightarrow \mathbb{R}$  is a positive definite kernel function defined on graphs [7], i.e. it is a similarity measure between graphs, which is symmetric and positive definite [20]. It is known that, if  $k$  is a graph kernel, there is a mapping  $\phi : \mathcal{G} \rightarrow \mathcal{H}$  from  $\mathcal{G}$  to some Hilbert space  $\mathcal{H}$ , such that  $k(g, g') = \langle \phi(g), \phi(g') \rangle_{\mathcal{H}}$  for all  $g, g' \in \mathcal{G}$ , where  $\langle \cdot, \cdot \rangle_{\mathcal{H}}$  denotes the inner product in  $\mathcal{H}$ . Therefore, graph kernels enable a feature space representation of graphs in the space  $\mathcal{H}$ , that allows the direct application of kernel methods, like support vector machines (SVMs), on the graph data. Such methods do not require the explicit representation of graphs in  $\mathcal{H}$ , but only the evaluation of the kernel function on pairs of graphs.

During the last years, several graph kernels have been proposed in the literature. Most of them are based on the ideas of decomposing graphs into smaller substructures and of building the kernel based on similarities between those components [7]. Following this approach, there are kernels based on different types of substructures, like walks [21], paths [22] and trees [23]. In this paper, we use the Shortest-path (SP) graph kernel [22] and the Weisfeiler-Lehman (WL) graph kernels [23], which have shown good practical performance and also have a low computational complexity. The SP kernel computes the similarity between pairs of graphs based on the number of similar shortest-paths between pairs of nodes in both graphs. On the other hand, the WL kernel computes the similarity based on common tree patterns that occur in both graphs.

These graph kernels measure the similarity between graphs based on differences in their global topology, in terms of paths and trees patterns. For this reason, they do not directly exploit the information based on one-to-one corre-

spondence between nodes across graphs, when available. When the task-related information is in systematic differences of the graph topology, the graph kernels are the correct tool to use. Conversely, when there is node correspondence, e.g. when nodes have anatomical meaning across graphs, the task-related information may be in the systematic differences in the weights of the edges and graph kernels may be inadequate to extract the desired information.

In this case, the explicit embedding of the graphs into a vector space is an alternative strategy that exploits the one-to-one node correspondence. Following this idea, the simpler approach is called Direct Connection Embedding (DCE) [3]. It is basically the computation of a feature vector by unfolding the upper triangular part of the adjacency matrix of each graph. Another embedding technique that has been used in this context was introduced in [3] and it is based on the dissimilarity representation approach for pattern recognition [24]. The idea is to create a vector representation of each graph based on its Euclidean distance to a set of predefined graphs (vectors), called prototypes. In our experiments, we call this method as Dissimilarity Representation Embedding (DRE). Both embedding techniques use the information related to the node correspondence, however they do not directly measure differences on the global topology of the graph.

In order to use kernel methods, like SVMs or the KTST, a kernel function must be available. Therefore, graph kernels like SP and WL can be directly used. On the other hand, embedding techniques like DCE and DRE can also be used by redefining them as kernel functions. This can be done by adding a kernel for vector data on the features obtained by the embedding. More formally, let  $e : \mathcal{G} \rightarrow \mathbb{R}^d$  be a graph embedding function, e.g. DCE, we can define the corresponding kernel function  $k_e : \mathcal{G} \times \mathcal{G} \rightarrow \mathbb{R}$  as

$$k_e(g, g') = k_v(e(g), e(g'))$$

where  $k_v$  is a kernel function for vector data, like the linear or Gaussian (RBF) kernels.

## 2.3 Hypothesis Testing

There are different schools of thought about testing hypotheses, which define different testing procedures. Here we adopt the Frequentist framework because it is the main one in the experimental neuroscience field. Moreover it is the one adopted both by CBT and KTST. Within the Frequentist framework, the two main schools of thought are those associated with Fisher [25] and Neyman-Pearson [26]. In our experiments, described in Section 4, we adopted both views for different purposes. For this reason, here we briefly report the two procedures and their aim.

### 2.3.1 Fisher significance testing

the procedure for testing hypotheses defined by Fisher [25], is based on the definition of the hypothesis to disprove with the experiment, i.e. the *null hypothesis*

$H_0$ , and by quantifying the evidence in the data against it. It comprises the following steps:

1. Set up the null hypothesis  $H_0$  to disprove.
2. Define an appropriate test statistic  $T$ , which is a function that, given the collected data, summarizes them in a real number.
3. Compute  $p(T|H_0)$ , i.e. the distribution of  $T$  when  $H_0$  is true, for example with resampling techniques.
4. Run the experiment, collect the data and compute  $T^*$  as the value of the test statistic for the observed data.
5. Compute the  $p$ -value =  $p(T \geq T^*|H_0)$ , as the probability of getting an equal or more extreme value of  $T^*$  when  $H_0$  is true.
6. Report the  $p$ -value as a quantification of the evidence against  $H_0$ .

The interpretation of the  $p$ -value as a measure of evidence against  $H_0$  has been subject to debate in the literature [27]. Nevertheless, it is common practice to define a threshold  $\theta$  for the  $p$ -value, below which the result is considered *significant*. Typical values for are  $\theta = 0.05$  or  $\theta = 0.01$ .

### 2.3.2 Neyman-Pearson hypothesis testing

the procedure to test hypotheses defined by Neyman and Pearson [26] is based on defining two alternative hypotheses and to decide which one to accept, by characterizing the test through the probability of Type I ( $\alpha$ ) and Type II ( $\beta$ ) error and the sample size  $N$ . These are the steps:

1. Set up two complementary hypotheses,  $H_0$  (null) and  $H_1$  (alternative).
2. Define an appropriate test statistic  $T$ .
3. Trade-off  $\alpha = p(\text{reject } H_0|H_0 \text{ is true})$ ,  $\beta = p(\text{reject } H_1|H_1 \text{ is true})$  and the sample size  $N$ , to fit the goals of the experiment.
4. Compute the rejection region(s)  $\mathcal{R}$  for  $T$ , where  $H_1$  is accepted and  $H_0$  rejected.
5. Run the experiment, collect the data and compute  $T^*$  as the value of the test statistic for the observed data.
6. Reject  $H_0$  and accept  $H_1$  if  $T^* \in \mathcal{R}$ . Or viceversa, if  $T^* \notin \mathcal{R}$ .

A test is called *consistent* if  $\beta \rightarrow 0$  as  $n \rightarrow \infty$  whenever  $H_0$  is false.

Common steps for the Fisher and Neyman-Pearson approaches are the definition of the test statistic and the derivation of its null distribution. In the following we describe this two steps for the CBT and the KTST.

## 2.4 Classification-Based Test

A classifier  $c \in \mathcal{C}$  is a function  $c : \mathcal{G} \mapsto \mathcal{Y}$  that returns the predicted class label given a graph. Typically classifiers need training to be instantiated. This requires that a portion of the dataset  $D$ , called train set  $D_{train}$ , is used to fit the classifier to the data.

In the classification-based test (CBT), i.e. when testing whether a classifier is able to discriminate the two classes  $\{a, b\}$ , the null hypothesis  $H_0$  is that  $c$  predicts at chance-level and the alternative hypothesis  $H_1$  is that  $c$  predicts better than chance-level<sup>1</sup>. The most common measure to quantify the ability of classifier to discriminate the classes is the generalization error  $\epsilon = E_{\mathcal{G} \times \mathcal{Y}}[I(Y, c(G))]$ , where  $I$  is the indicator function. The standard unbiased estimator of  $\epsilon$  is the *error rate*  $\hat{\epsilon} = \frac{1}{|D_{test}|} \sum_{(g,y) \in D_{test}} I(y, c(g))$ , where  $D_{test} = D \setminus D_{train}$ . Here we adopt the complementary measure of the error rate, i.e. *accuracy*  $acc = 1 - \hat{\epsilon}$ , which is more common in neuroscience applications.

When  $D_{test}$  is imbalanced, i.e. when  $n$  and  $m$  considerably differ, the interpretation of accuracy as a measure of discrimination, can be problematic [29, 30]. An alternative measure that reduces the impact of this problem is *balanced accuracy* [29], i.e. the average per-class accuracy  $acc_B = \frac{1}{2} \left( \frac{TP}{m} + \frac{TN}{n} \right)$ , where  $TP$ ,  $TN$  are the true negatives and true positives, i.e. the correctly classified examples of class  $A$  and  $B$ , respectively. Notice that, for  $acc_B$ , the chance level is always 0.5, irrespective of how imbalanced the data are.

The estimation of performance measure like  $acc$  or  $acc_B$  may have high variability for small  $N$ . Moreover, the split of  $D$  in  $D_{train}$  and  $D_{test}$  is stochastic, adding more variability to the estimate. In order to reduce this issue, it is common to adopt a resampling technique, the most common in this context being  $\kappa$ -folds cross-validation (CV). In CV,  $D$  is randomly split in  $\kappa$  non-overlapping parts and, iteratively, one is used as test set and the remaining parts as train set. The cross-validated balanced accuracy,  $acc_{CV}$ , is then the average  $acc_B$  across the folds.

In practical cases, most classifiers have additional parameters, called hyperparameters, that must be set before training, e.g. the regularization term of SVMs. For this reason, part of the data need to be used to assess such parameters. In order to avoid circularity, care has to be taken in selecting the portion of the data for this step. The standard process for unbiased estimation of hyperparameters, training and estimation of the error rate requires a nested CV scheme, as described in [31]. Notice that hyperparameter estimation, training and error rate estimation compete in the exclusive use of the data, because the more the data is used for one, the less remain for the others. The effect of this competition is further uncertainty in the estimates, which may reach critical levels for small  $N$ .

In the CBT, the usual test statistic  $T$  is  $acc_{CV}$ . In practical cases, the null distribution of  $acc_{CV}$  is estimated through resampling, specifically through permutations of the class labels in  $D$ . In this work we adopt the standard Monte

<sup>1</sup>In this work we do not discuss *antilearning* [28], the rare event where the classifier performs systematically worse than chance.

Carlo approximation of the permutation approach in which, for  $M$  iterations, the examples are randomly assigned the group  $A$  or  $B$  and the permuted  $acc_{CV}$  is computed. The null distribution of  $acc_{CV}$  is then approximated by the obtained  $M$  values. The approximated  $p$ -value of the observed (unpermuted)  $acc_{CV}^*$  is then the fraction of the  $M$  values greater than  $acc_{CV}^*$ .

Given  $\kappa$  folds,  $v$  hyperparameter values and  $M$  permutations, the computational cost of CBT is dominated by the  $Mv\kappa^2$  trainings and testings for the estimation of the null distribution, because of the nested cross-validation for each permutation and because in the inner loop all hyperparameters are attempted. Notice that, usually, training and testing are computationally expensive and even for small datasets CBT may require a large amount of time to be computed.

## 2.5 Kernel Two-Sample Test

A two-sample problem compares samples from two probability distributions  $P_A$  and  $P_B$ . A two-sample test is an hypothesis test where the null hypothesis  $H_0 : P_A = P_B$  and the alternative hypothesis  $H_1 : P_A \neq P_B$  are tested given the data.

Two sample tests can be parametric, like the Student’s  $t$ -test in one dimension or the Hotelling  $T$ -test in higher dimensions, where  $P_A$  and  $P_B$  are Gaussians. These tests do not directly apply to graphs because they require real values or vectors. Moreover, in the high-dimensional setting, e.g. the one obtained through graph embedding, the  $T$ -test performs poorly, as explained in [32].

To address the high-dimensional setting or more general topological spaces, some non-parametric two-sample tests have been proposed in the literature. For a brief review see [17] Section 3.3. Among them, the most popular one is the kernel two-sample test (KTST) [16, 17] which is based on the *maximum mean discrepancy* (MMD) test statistic:

$$\text{MMD}[P_A, P_B] = \max_{\|f\|_{\mathcal{H}} \leq 1} (E_{P_A}[f(x_A)] - E_{P_B}[f(x_B)]) \quad (1)$$

where the function  $f$  is from the unit ball in a reproducing kernel Hilbert space  $\mathcal{H}$  and  $x_A, x_B \in \mathcal{X}$  are objects from a generic topological space  $\mathcal{X}$ , sampled according to  $P_A$  or  $P_B$ . Notice that  $x$  is not necessarily a vector but can be any object, like a graph, for which  $\mathcal{H}$  is defined. As mentioned in Section 2.2,  $\mathcal{H}$  can be defined through a kernel function  $k(x, x') : \mathcal{X} \times \mathcal{X} \mapsto \mathbb{R}$ . In [17], an interesting property of MMD is proved: for some families of kernels called *characteristic* kernels, like the Gaussian and Laplacian kernels [33],

$$\text{MMD}[P_A, P_B] = 0 \quad \text{if and only if} \quad P_A = P_B.$$

when  $k$  is bounded. This result means that the KTST is consistent for such kernels. In [17] the following relationship between MMD and the given kernel



is derived:

$$\begin{aligned} \text{MMD}^2[P_A, P_B] = & E_{x_A, x'_A}[k(x_A, x'_A)] + \\ & - 2E_{x_A, x_B}[k(x_A, x_B)] + \\ & + E_{x_B, x'_B}[k(x_B, x'_B)] \end{aligned} \quad (2)$$

In practical cases, we do not have access to  $P_A$  and  $P_B$ , but just to the samples  $A$  and  $B$ . In [17], an unbiased estimate of  $\text{MMD}^2$  is derived

$$\begin{aligned} \text{MMD}_u^2(A, B) = & \frac{1}{m(m-1)} \sum_{i \neq j} k(x_i^A, x_j^A) + \\ & - \frac{2}{mn} \sum_{i, j} k(x_i^A, x_j^B) + \\ & + \frac{1}{n(n-1)} \sum_{i \neq j} k(x_i^B, x_j^B) \end{aligned} \quad (3)$$

Notice that  $\text{MMD}$  and  $\text{MMD}_u^2$  are not absolute measures of the differences between two distributions. For example, if we use two different kernels on the same data / distributions, we cannot numerically compare the two  $\text{MMD}_u^2$ . The same issue occurs when computing  $\text{MMD}$  from two different problems, pertaining to different domains and distributions. From this point of view, in the context of experimental neuroscience described here,  $\text{MMD}$  cannot be used as a measure of the *effect size* of the phenomenon under investigation.

The null distribution of  $\text{MMD}_u^2$  can be estimated in different ways, as described in [17]. In case of small samples, which is typical of the neuroimaging domain, a resampling approach is suggested, which here we implement as permutation test. In this work we adopt the standard approximation of the permutation test, as described for the CBT in Section 2.4. This requires computing  $\text{MMD}_u^2$  for each of the  $M$  permutations, for some large  $M$ , e.g.  $M = 10000$ ,

Given  $N$  subjects/examples,  $M$  permutations and assuming that the kernel matrix  $K = [k(x_i, x_j)]_{i, j=1 \dots N}$  is precomputed in advance, the computational cost of the KTST is approximately of  $MN^2$  sums.

### 3 Materials

In this section we describe the datasets used in the experiments of Section 4.

#### 3.1 1000 Functional Connectomes Dataset

The first dataset corresponds to the connectivity matrices computed from the resting state fMRI data acquired under the 1000 Functional Connectome Project<sup>2</sup>.

<sup>2</sup>[http://www.nitrc.org/projects/fcon\\_1000](http://www.nitrc.org/projects/fcon_1000)

This dataset is publicly available [34], and particularly, the functional connectivity matrices can be downloaded from the USC Multimodal Connectivity Database [35] under the name *1000\_Functional\_Connectomes*<sup>3</sup>.

We use this dataset for a gender classification problem, i.e.  $\mathcal{Y} = \{\text{male, female}\}$ , motivated by a similar experiment in [36]. In this dataset, all brain data was motion-corrected and normalized to a standard template where 177 brain regions were defined. Therefore, all graphs are composed of  $|V| = 177$  nodes, and it is possible to establish the correspondence between nodes representing the same brain region.

This dataset is a collection of fMRI datasets recorded at different locations all over the world. In our experiments, we grouped the data according their location and each location-specific dataset was used independently, to avoid batch effects due to different MRI scanners. Additionally, we discarded the locations-specific datasets with too few subjects, i.e. when either  $m < 10$  or  $n < 10$ . In such cases, it is expected that both CBT and KTST are not able to reject  $H_0$  when it is indeed false, just for lack of data. By discarding those excessively small datasets, we avoided to include cases where the agreement between CBT and KTST was granted because of the sample size and not because of the actual information content in the data. In other words, we carefully prevented to artificially inflate the claimed agreement between CBT and KTST.

In this way, this large dataset is transformed into 12 smaller datasets, each one containing the data of a specific location. The name of the remaining locations and their corresponding number of subjects per class is reported in Table 1.

## 3.2 Schizophrenia Dataset

We used the functional connectivity dataset released with the MLSP 2014 Schizophrenia Classification Challenge<sup>4</sup>. This data is partially described in [37]. The dataset is composed by 86 functional connectivity matrices,  $m = 46$  belonging to the control class and  $n = 40$  to the schizophrenia class. The brain data of all subjects was parcelled into 28 regions and therefore all graphs have  $|V| = 28$  nodes, and the node correspondence could be established. The weights on the edges correspond to the correlation between time series of every pair of brain regions.

## 3.3 Contextual Disorder Dataset

The third dataset corresponds to a listening task experiment with fMRI data recently proposed in [38]. In this study, 19 healthy participants were presented with two types of sequences of auditory stimuli:  $\mathcal{Y} = \{\text{ordered, disordered}\}$ , as well as two other conditions not discussed here. Each sequence, of 150s, was presented once to each participant, therefore the dataset is composed of 38 examples. Connectivity graphs were computed by following the approach

<sup>3</sup>[http://umcd.humanconnectomeproject.org/umcd/default/browse\\_studies](http://umcd.humanconnectomeproject.org/umcd/default/browse_studies)

<sup>4</sup><http://www.kaggle.com/c/mlsp-2014-mri/data>

presented in [12]. First, a hierarchical clustering algorithm was independently applied on each participant’s data in order to define brain regions, i.e. the nodes the graph. Then, correlation values between the average timeseries of the pairs of regions were used to define the edge weights.

In this dataset the data of different participants were processed independently. Therefore, graphs computed from different participants had different number of nodes and there was no anatomical correspondence between any pair of nodes across the graphs.

### 3.4 Simulated Data

We generated multiple simulated datasets each consisting of  $m = n = 20$  star graphs with  $d + 1$  nodes and  $d$  edges. We assumed node correspondence and defined  $P_A$  and  $P_B$  as  $d$ -dimensional multivariate normal distributions of weights of the edges.  $P_A$  and  $P_B$  had same covariance but different mean:  $\mu_A = (0, \dots, 0) \in \mathbb{R}^d$ ,  $\mu_B = (\delta, \dots, \delta) \in \mathbb{R}^d$ , thus  $\delta$  was the effect size. We generated 1000 datasets with  $d = 5$  and  $\delta \in \{0.0, 0.25, 0.5, 0.75, 1.0\}$ , simulating both cases, i.e when  $H_0 : P_A = P_B$  ( $\delta = 0$ ) is true and when  $H_0$  is false ( $\delta \in \{0.25, 0.5, 0.75, 1.0\}$ ), with different effect sizes.

## 4 Experiments

With a set of experiments, we investigated the degree of agreement between KTST and CBT, to see whether KTST is a viable alternative to CBT. In order to do that, in this section we show the results of CBT and KTST on 14 datasets, spanning different scientific questions and using two graph embeddings (when possible) and two graph kernels. This section is concluded with a simulation study where, on a simplified example, the probability of Type I and Type II error is quantified both for CBT and KTST, for sample sizes analogous to those of typical neuroimaging experiments.

In all experiments, in order to avoid biases and to keep the experimental conditions most similar between CBT and KTST, we used SVMs as classifier<sup>5</sup> so to use the same kernel matrix for CBT and KTST. The kernel matrices related to graph embeddings were based on the Gaussian kernel, as mentioned in Section 2.2, using the median value of the distances between the graphs, as the  $\sigma$  parameter. This is a standard heuristic in case of low sample size, because it avoids spending class-labeled data to fit  $\sigma$ . All kernel matrices of all experiments were pre-computed in advance.

The CBT test statistic was the 5-fold cross-validated balanced accuracy  $acc_{CV}$  in all cases. The null distributions of  $acc_{CV}$  and  $MMD_u^2$  were approximated with  $M = 10000$  permutations. As noted in Section 2.4, the actual value of  $acc_{CV}$  depends on the random train/test split during the (nested) cross-validation process, which introduces variability in the result. In the following,

<sup>5</sup>For model selection, the regularization parameter of SVM was optimized over  $v = 25$  values ranging from  $10^{-5}$  to  $10^5$ , equally spaced in log-scale.

in Table 1 and Figure 1, we report the *median*  $acc_{CV}$  and its related  $p$ -value after 100 repetitions of the estimation process. Differently, the  $MMD_u^2$  value is deterministic and has no such variability.

In Figure 2, 3, 4 and 5 we explicitly show the variability of the  $p$ -values associated to the multiple estimates of  $acc_{CV}$  through boxplots, because this is an important element for the discussion in Section 5.

We report that, in each single test, the time to compute CBT and KTST greatly differed, according to what was mentioned in Section 2.4 and Section 2.5. In the typical case of  $m = n = 30$ , CBT required hours of computation on a modern 4-cores computer, while KTST required just a few seconds.

#### 4.1 Agreement between CBT and KTST

We carried out the CBT and KTST on the brain graphs from 14 datasets, coming from three different scientific studies: the 1000 Functional connectome, a schizophrenia study and a cognitive neuroscience study about processing ordered and unordered sequences of auditory stimuli. In Section 3 are reported the details of each study. Here we mention that, in the first two studies, the data is preprocessed in order to provide node correspondence, which is ideal for graph embeddings, while in the third study there is no node correspondence, which allows the use of only graph kernels.

From the first study, i.e. the 1000 Functional Connectome, we analyzed 12 dataset from different recording locations in order to investigate their relation to the gender of the subject. In these dataset, the size of the subgroups, i.e. male and female, ranges from 10 to 123. The second study, about schizophrenia, comprises 40 patients and 46 healthy controls. The third study, about ordered and unordered auditory stimuli, provides data from 19 subjects, each with one recording session for both categories of stimulus.

In Table 1, for each dataset, we report the size of each dataset ( $n$  and  $m$ ), the balanced accuracy  $acc_{CV}$  and the  $p$ -values of CBT and KTST for two different graph embeddings, i.e. DCE and DRE, and for two different graph kernels, i.e. WL and SP, as explained in Section 2.2.

In Figure 1 we plot the results of Table 1 in log-log scale, to show the agreement between CBT and KTST. There, each location is represented as point with coordinates given by the  $p$ -value of CBT and  $p$ -value of KTST, and different colors are used for different embeddings or kernels.

As mentioned before, in Figure 2, 3 and 4 we explicitly show the variability of the  $p$ -values associated to the multiple estimates of  $acc_{CV}$ , through boxplots, for each of the 14 datasets. We do not report equivalent boxplots for the  $p$ -values of KTST because  $MMD_u^2$  is deterministic and the only (negligible) source of variability was the approximation of the null distribution. With  $M = 10000$  iterations, those  $p$ -values were always stable to the reported 3rd decimal place.

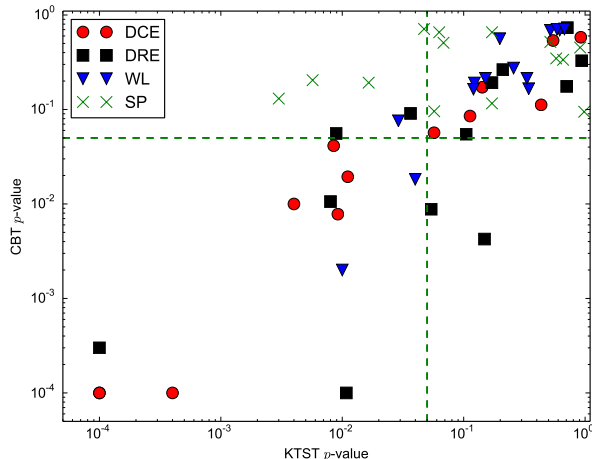


Figure 1: Results of Table 1 represented as the  $p$ -value of KTST vs. the  $p$ -value of CBT. Each point corresponds to a dataset and the shape/color represents the embedding or kernel used. The horizontal dashed lines are the thresholds for significance  $\theta = 0.05$ .

## 4.2 Simulation: Type I and II error for Low Sample Size

We conducted a simulation study to quantify the probability of Type I error and Type II error, for CBT and KTST, in the low sample size regime, in order to characterize the tests according to the Neyman-Pearson paradigm (see Section 2.3.2). Here we expected that the various sources of variability in the estimation process of CBT, described in Section 2.4, had a negative impact, increasing the number of errors with respect to that of KTST. The datasets used are generated according to the description in Section 3.4.

In the first part of the simulation, we used the dataset for which  $H_0$  is true ( $\delta = 0.0$ ). Here we quantified  $p(\text{Type I})$ , i.e.  $H_0$  true but rejected, for CBT and KTST using the DCE embedding and Gaussian kernel on the sampled graphs. In the same way, in the second part of the simulation, we used the datasets for which  $H_0$  is false with different degrees of the effect size ( $\delta \in \{0.25, 0.5, 0.75, 1.0\}$ ). With the second part we quantified  $p(\text{Type II})$ , i.e.  $H_0$  false but not rejected. The results over 1000 repetitions are reported in Table 2.

## 4.3 Reproducibility of the Results

All the code used in the experiments and in the simulation study, that generates the tables and the figures in this section, was developed in Python using the numerical libraries NumPy and SciPy, together with the machine learning package Scikit-learn [39]. Our code is available under a Free / OpenSource license

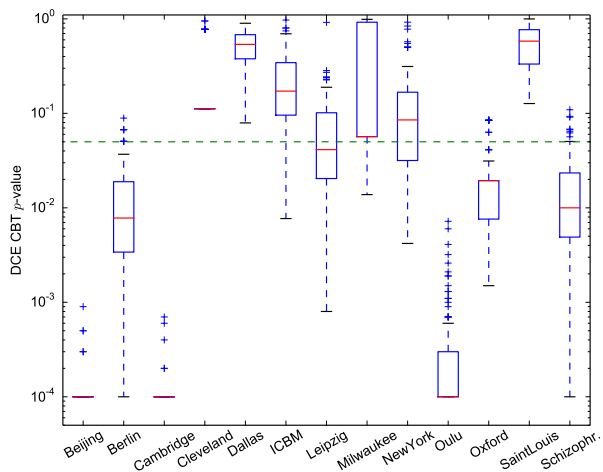


Figure 2: For each dataset of the experiments, the boxplots represent the variability of the  $p$ -values of CBT with DCE across multiple runs. The horizontal dashed line is the threshold for significance  $\theta = 0.05$ .

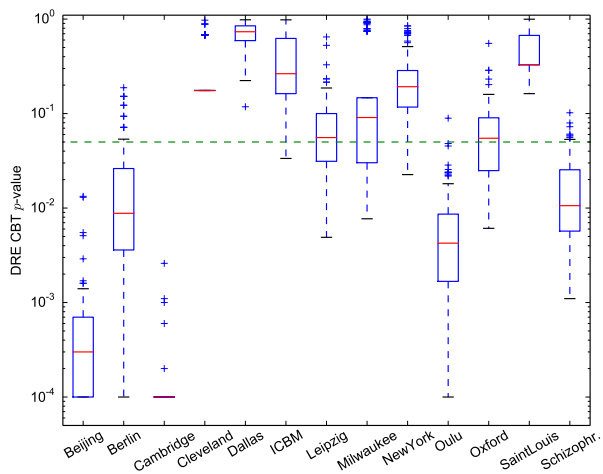


Figure 3: For each dataset of the experiments, the boxplots represent the variability of the  $p$ -values of CBT with DRE across multiple runs. The horizontal dashed line is the threshold for significance  $\theta = 0.05$ .

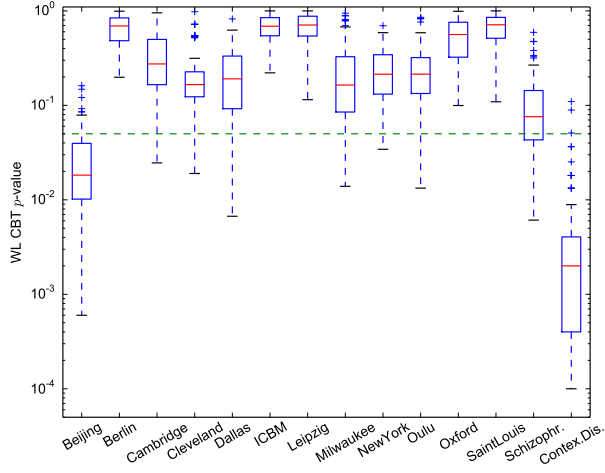


Figure 4: For each dataset of the experiments, the boxplots represent the variability of the  $p$ -values of CBT with the WL kernel across multiple runs. The horizontal dashed line is the threshold for significance  $\theta = 0.05$ .

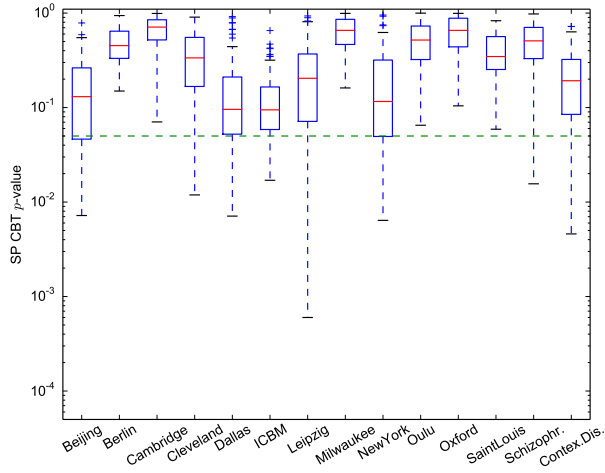


Figure 5: For each dataset of the experiments, the boxplots represent the variability of the  $p$ -values of CBT with SP kernel across multiple runs. The horizontal dashed line is the threshold for significance  $\theta = 0.05$ .

at <https://github.com/emanuele/jstsp2015>.

## 5 Discussion

Table 1 and Figure 1 show a strong agreement between the  $p$ -values of CBT and KTST across all datasets, supporting the claim of equivalent results between the two approaches. The Spearman correlation coefficient between all the 54 pairs of  $p$ -values of CBT and KTST is 0.79 ( $p$ -value  $< 0.00001$ )<sup>6</sup>, which is highly significant. Notice that this result holds across multiple datasets from different domains and using both graph embeddings and graph kernels.

Considering a standard threshold  $\theta = 0.05$  to declare the  $p$ -value as significant, in Table 1 there are 45 cases of agreement between CBT and KTST, i.e. when either both rejected  $H_0$  or both did not. The 9 cases of disagreement, i.e. when the CBT did not reject  $H_0$  while the KTST did (or viceversa), are reported in Table 1 in bold font. These cases occur for DRE (Berlin, Leipzig, Milwaukee and Oulu), WL (Schizophrenia) and SP (Beijing, Cambridge, Leipzig, and Contextual Disorder). For those cases, it is enlightening to see Figure 3, 4 and 5, where, for each dataset, the great variability of  $acc_{CV}$  is represented in the great variability of the associated  $p$ -values, always ranging from significant values to non-significant ones. From those figures, we can safely conclude that the disagreement is dominated by variability of CBT and not by inherent disagreement between CBT and KTST.

In Figure 2, 3, 4 and 5 it is shown the great variability of the  $p$ -values obtained with 100 repetitions of the CBT. This variability is due to the variability of the  $acc_{CV}$  estimate, occurring because of the non-deterministic train/test split during cross-validation and because of the competing joint fit of the classifier against the estimation of the hyperparameters during model selection. See Section 2.4 for the detailed explanation. Conversely, for KTST, the estimate of  $MMD_u^2$  has no variability because it is deterministic, given the data. The variability of its associated  $p$ -value is due only to the approximation of the null distribution through permutations. Such variability can be controlled to the desired level and was negligible with  $M = 10000$  permutations in all experiments. The much greater variability of CBT with respect to KTST is a clear advantage in favor of the proposed test.

In Section 4.2, the effect of the great variability of CBT in the regime of low sample size is studied with a simulation, in order to quantify the impact in terms of Type I and Type II error, in a simplified setting. The results reported in Table 2 show that when the null hypothesis  $H_0$  is true, i.e. the effect size  $\delta = 0$ , the rate of false discovery, i.e. the frequency of Type I error, is almost equivalent for CBT and KTST, with a marginal 2% advantage in favor of KTST, both when the significance threshold is  $\theta = 0.05$  or  $\theta = 0.01$ . When  $H_0$  is false, i.e. when  $\delta > 0$ , the sensitivity of CBT and KTST, in terms of frequency of Type II error, is computed and reported in Table 2. As expected, when the effect size is too low or too high, i.e.  $\delta = 0.25$  and  $\delta = 1.0$  respectively, both

<sup>6</sup>Estimated with a permutation test and 10000 permutations.



CBT and KTST behaves similarly. But in the intermediate cases, i.e. when  $\delta = 0.5$  and  $\delta = 0.75$ , the advantage of KTST becomes much greater, ranging from 7% to 20% reduction of the Type II error. This results clearly confirms that KTST is more sensitive than CBT for low sample size, at least in some cases, and equivalent in other cases. Notice that analogous results can be obtained when changing the dimension  $d$  of the simulated datasets and after adjusting the effect size  $\delta$  accordingly.

As reported in Section 4, computing the CBT required hours while KTST required only a few seconds. This is expected given the description of the amount of the respective computation in Section 2.4 and Section 2.5, at least in the setting of our experiments, i.e. low  $N$ , which is typical for neuroimaging data. Almost all the time of the computation is used for the Monte Carlo approximation of the null distribution, during which the respective test statistics,  $acc_{CV}$  and  $MMD_u^2$ , are estimated  $M = 10000$  times. Estimating  $acc_{CV}$  is approximately 1000 times slower than estimating  $MMD_u^2$ , because  $acc_{CV}$  is a nested loop, where a classifier is trained and tested at each iteration. Moreover, in the internal loop, training and testing is done for each of the hyperparameter values. Notice that training a classifier usually requires to solve an optimization problem, so a large number of costly optimizations are necessary. Conversely,  $MMD_u^2$  requires only  $N^2$  sums. This is another clear advantage of KTST over CBT.

## 6 Conclusions

In this work we proposed the use of the kernel two-sample test (KTST) for studying systematic differences between two population of graphs representing brain networks. We compared the KTST with the common use of classifiers, that here we call classification-based test (CBT). We claimed that, in general, both tests provide very similar results and, in Section 4, we showed it in practice, with multiple experiments.

We also explained that, for low sample size, the result of CBT may present high variability *on the same dataset* and gave detailed description of the causes in Section 2.4. This is a major difference with respect to KTST, which instead has no (or negligible) variability, given the data. This difference between the two tests is the motivation of the increased Type II error of CBT with respect to KTST, that we studied with a simulation presented in Section 4.2. A partial remedy to the instability of the result of CBT is to estimate multiple times  $acc_{CV}$ , instead of just once, and to report the median value. This remedy increases the amount of computations required by the CBT, which is already more than 1000 times greater than those for the KTST, i.e. hours vs. seconds.

One limitation of KTST is the lack of an absolute measure of the effect size in the data, which means that the KTST can be used to quantify the significance of a phenomenon but not its effect size. The MMD test statistics is not an absolute measure of distance between distributions, in the sense that, in general, the MMD value from two different problems cannot be directly compared. This

is different from the CBT, where performance measures of the classifier, like accuracy, have an absolute meaning. For this reason, as a final conclusion, we do not propose to reject the use of classifiers in the domain of brain networks, but to use both KTST and classifiers to study significance and effect size, respectively.

As future work, we plan to investigate the characteristic property of graph kernels, which, up to now, has never been proved. As mentioned in Section 2.5, a *consistent* KTST requires a characteristic graph kernel. Anyway, this is not very different from using a kernel based on graph embedding plus the Gaussian kernel, as we do in this study. Even though the Gaussian kernel is characteristic, no results are known about mixing it with graph embeddings. Notice that, to the best of our knowledge, also the consistency of the CBT has never been proved.

## References

- [1] K. Supekar, V. Menon, D. Rubin, M. Musen, and M. D. Greicius, “Network Analysis of Intrinsic Functional Brain Connectivity in Alzheimer’s Disease,” *PLoS Comput Biol*, vol. 4, no. 6, pp. e1000100+, Jun. 2008. [Online]. Available: <http://dx.doi.org/10.1371/journal.pcbi.1000100>
- [2] D. S. Bassett, B. G. Nelson, B. A. Mueller, J. Camchong, and K. O. Lim, “Altered resting state complexity in schizophrenia.” *NeuroImage*, vol. 59, no. 3, pp. 2196–2207, Feb. 2012. [Online]. Available: <http://view.ncbi.nlm.nih.gov/pubmed/22008374>
- [3] J. Richiardi, D. Van De Ville, K. Riesen, and H. Bunke, “Vector Space Embedding of Undirected Graphs with Fixed-cardinality Vertex Sequences for Classification,” in *Pattern Recognition (ICPR), 2010 20th International Conference on*. IEEE, Aug. 2010, pp. 902–905. [Online]. Available: <http://dx.doi.org/10.1109/icpr.2010.227>
- [4] E. Tagliazucchi, F. von Wegner, A. Morzelewski, S. Borisov, K. Jahnke, and H. Laufs, “Automatic sleep staging using fMRI functional connectivity data,” *NeuroImage*, vol. 63, no. 1, pp. 63–72, Oct. 2012. [Online]. Available: <http://dx.doi.org/10.1016/j.neuroimage.2012.06.036>
- [5] J. Richiardi and B. Ng, “Recent advances in supervised learning for brain graph classification,” in *Global Conference on Signal and Information Processing (GlobalSIP), 2013 IEEE*. IEEE, Dec. 2013, pp. 907–910. [Online]. Available: <http://dx.doi.org/10.1109/globalsip.2013.6737039>
- [6] J. Richiardi, S. Achard, H. Bunke, and D. Van De Ville, “Machine Learning with Brain Graphs: Predictive Modeling Approaches for Functional Imaging in Systems Neuroscience,” *Signal Processing Magazine, IEEE*, vol. 30, no. 3, pp. 58–70, May 2013. [Online]. Available: <http://dx.doi.org/10.1109/msp.2012.2233865>

- [7] S. V. N. Vishwanathan, N. N. Schraudolph, R. Kondor, and K. M. Borgwardt, “Graph Kernels,” *J. Mach. Learn. Res.*, vol. 11, pp. 1201–1242, Aug. 2010. [Online]. Available: <http://portal.acm.org/citation.cfm?id=1859891>
- [8] Y. Fu and Y. Ma. (2013) Graph embedding for pattern analysis. [Online]. Available: <http://www.worldcat.org/isbn/9781461444572>
- [9] F. Mokhtari and G.-A. A. Hossein-Zadeh, “Decoding brain states using backward edge elimination and graph kernels in fMRI connectivity networks.” *Journal of neuroscience methods*, vol. 212, no. 2, pp. 259–268, Jan. 2013. [Online]. Available: <http://dx.doi.org/10.1016/j.jneumeth.2012.10.012>
- [10] S. Takerkart, G. Auzias, B. Thirion, D. Schön, and L. Ralaivola, “Graph-Based Inter-subject Classification of Local fMRI Patterns,” in *Machine Learning in Medical Imaging*, ser. Lecture Notes in Computer Science, F. Wang, D. Shen, P. Yan, and K. Suzuki, Eds. Springer Berlin Heidelberg, 2012, vol. 7588, pp. 184–192. [Online]. Available: [http://dx.doi.org/10.1007/978-3-642-35428-1\\_23](http://dx.doi.org/10.1007/978-3-642-35428-1_23)
- [11] S. Vega-Pons and P. Avesani, “Brain Decoding via Graph Kernels,” in *Pattern Recognition in Neuroimaging (PRNI), 2013 International Workshop on*. IEEE, Jun. 2013, pp. 136–139. [Online]. Available: <http://dx.doi.org/10.1109/prni.2013.43>
- [12] S. Vega-Pons, P. Avesani, M. Andric, and U. Hasson, “Classification of inter-subject fMRI data based on graph kernels,” in *Pattern Recognition in Neuroimaging, 2014 International Workshop on*. IEEE, Jun. 2014, pp. 1–4. [Online]. Available: <http://dx.doi.org/10.1109/prni.2014.6858549>
- [13] B. Jie, D. Zhang, C.-Y. Wee, and D. Shen, “Topological graph kernel on multiple thresholded functional connectivity networks for mild cognitive impairment classification,” *Hum. Brain Mapp.*, vol. 35, no. 7, pp. 2876–2897, Jul. 2014. [Online]. Available: <http://dx.doi.org/10.1002/hbm.22353>
- [14] J. Richiardi, H. Eryilmaz, S. Schwartz, P. Vuilleumier, and D. Van De Ville, “Decoding brain states from fMRI connectivity graphs.” *NeuroImage*, vol. 56, no. 2, pp. 616–626, May 2011. [Online]. Available: <http://dx.doi.org/10.1016/j.neuroimage.2010.05.081>
- [15] F. Pereira, T. Mitchell, and M. Botvinick, “Machine learning classifiers and fMRI: a tutorial overview,” *Neuroimage*, vol. 45, no. 1, pp. S199–S209, 2009.
- [16] A. Gretton, K. M. Borgwardt, M. Rasch, B. Schölkopf, and A. J. Smola, “A Kernel Method for the Two-Sample-Problem,” in *NIPS*, 2006. [Online]. Available: [http://books.nips.cc/papers/files/nips19/NIPS2006\\_0583.pdf](http://books.nips.cc/papers/files/nips19/NIPS2006_0583.pdf)

- [17] A. Gretton, K. M. Borgwardt, M. J. Rasch, B. Schölkopf, and A. Smola, “A Kernel Two-Sample Test,” *Journal of Machine Learning Research*, 2012. [Online]. Available: <http://www.jmlr.org/papers/volume13/gretton12a/gretton12a.pdf>
- [18] E. Olivetti, D. Benozzo, S. M. Kia, M. Ellero, and T. Hartmann, “The Kernel Two-Sample Test vs. Brain Decoding,” in *Proceedings of the 2013 International Workshop on Pattern Recognition in Neuroimaging*, ser. PRNI '13. Washington, DC, USA: IEEE Computer Society, Jun. 2013, pp. 128–131. [Online]. Available: <http://dx.doi.org/10.1109/prni.2013.41>
- [19] E. Olivetti, S. M. Kia, and P. Avesani, “Sensor-level Maps with the Kernel Two-Sample Test,” in *Pattern Recognition in NeuroImaging, 2014 International Workshop on*. IEEE, Jun. 2014, pp. 1–4. [Online]. Available: <http://dx.doi.org/10.1109/PRNI.2014.6858537>
- [20] T. Hofmann, B. Schölkopf, and A. J. Smola, “Kernel methods in machine learning,” *Annals of Statistics*, vol. 36, no. 3, pp. 1171–1220, 2008. [Online]. Available: <http://projecteuclid.org/DPubS?service=UI&#38;version=1.0&#38;verb=Display&#38;handle=euclid.aos/1211819561>
- [21] H. Kashima, K. Tsuda, and A. Inokuchi, “Marginalized kernels between labeled graphs,” in *Proceedings of the Twentieth International Conference on Machine Learning*, 2003, pp. 321–328. [Online]. Available: <http://citeseerx.ist.psu.edu/viewdoc/summary?doi=10.1.1.90.7556>
- [22] K. M. Borgwardt and H. P. Kriegel, “Shortest-path kernels on graphs,” in *Data Mining, Fifth IEEE International Conference on*. IEEE, Nov. 2005, pp. 8 pp.–81. [Online]. Available: <http://dx.doi.org/10.1109/icdm.2005.132>
- [23] N. Shervashidze, P. Schweitzer, E. J. van Leeuwen, K. Mehlhorn, and K. M. Borgwardt, “Weisfeiler-Lehman Graph Kernels,” *J. Mach. Learn. Res.*, vol. 12, pp. 2539–2561, Nov. 2011. [Online]. Available: <http://portal.acm.org/citation.cfm?id=2078187>
- [24] E. Pekalska and R. P. W. Duin, *The Dissimilarity Representation for Pattern Recognition: Foundations And Applications (Machine Perception and Artificial Intelligence)*. World Scientific Publishing Company, Dec. 2005. [Online]. Available: <http://www.worldcat.org/isbn/9812565302>
- [25] R. A. Fisher, *The design of experiments*, 6th ed. Hafner Pub. Co, 1935.
- [26] J. Neyman and E. S. Pearson, “On the Problem of the Most Efficient Tests of Statistical Hypotheses,” *Philosophical Transactions of the Royal Society of London. Series A, Containing Papers of a Mathematical or Physical Character*, vol. 231, pp. 289–337, 1933. [Online]. Available: <http://dx.doi.org/10.2307/91247>

- [27] T. Sellke, M. J. Bayarri, and J. O. Berger, “Calibration of p Values for Testing Precise Null Hypotheses,” *The American Statistician*, vol. 55, no. 1, pp. 62–71, 2001. [Online]. Available: <http://dx.doi.org/10.2307/2685531>
- [28] A. Kowalczyk and O. Chapelle, “An Analysis of the Anti-learning Phenomenon for the Class Symmetric Polyhedron,” in *Algorithmic Learning Theory*, ser. Lecture Notes in Computer Science, S. Jain, H. I. r. i. c. h. Simon, and E. Tomita, Eds. Berlin, Heidelberg: Springer Berlin / Heidelberg, 2005, vol. 3734, ch. 8, pp. 78–91. [Online]. Available: [http://dx.doi.org/10.1007/11564089\\_8](http://dx.doi.org/10.1007/11564089_8)
- [29] K. H. Brodersen, C. S. Ong, K. E. Stephan, and J. M. Buhmann, “The Balanced Accuracy and Its Posterior Distribution,” in *Pattern Recognition (ICPR), 2010 20th International Conference on*. IEEE, Aug. 2010, pp. 3121–3124. [Online]. Available: <http://dx.doi.org/10.1109/icpr.2010.764>
- [30] E. Olivetti, S. Greiner, and P. Avesani, *Induction in Neuroscience with Classification: Issues and Solutions*, ser. Lecture Notes in Computer Science. Springer, 2012, vol. 7263, pp. 42–50. [Online]. Available: [http://dx.doi.org/10.1007/978-3-642-34713-9\\_6](http://dx.doi.org/10.1007/978-3-642-34713-9_6)
- [31] E. Olivetti, A. Mognon, S. Greiner, and P. Avesani, “Brain Decoding: Biases in Error Estimation,” *Brain Decoding: Pattern Recognition Challenges in Neuroimaging, Workshop on*, vol. 0, pp. 40–43, Aug. 2010. [Online]. Available: <http://dx.doi.org/10.1109/wbd.2010.9>
- [32] Z. D. Bai and H. Saranadasa, “Effect of high dimension: by an example of a two sample problem,” *Statistica Sinica*, vol. 6, pp. 311–329, 1996. [Online]. Available: <http://www3.stat.sinica.edu.tw/statistica/j6n2/j6n21/j6n21.htm>
- [33] K. Fukumizu, A. Gretton, X. Sun, and B. Schölkopf, “Kernel Measures of Conditional Dependence,” in *Advances in neural information processing systems 20*, Max-Planck-Gesellschaft. Red Hook, NY, USA: Curran, Sep. 2008, pp. 489–496. [Online]. Available: <http://papers.nips.cc/paper/3340-kernel-measures-of-conditional-dependence-supplemental.zip>
- [34] B. B. Biswal, M. Mennes, X.-N. N. Zuo, S. Gohel, C. Kelly, S. M. Smith, C. F. Beckmann, J. S. Adelstein, R. L. Buckner, S. Colcombe, A.-M. M. Dogonowski, M. Ernst, D. Fair, M. Hampson, M. J. Hoptman, J. S. Hyde, V. J. Kiviniemi, R. Kötter, S.-J. J. Li, C.-P. P. Lin, M. J. Lowe, C. Mackay, D. J. Madden, K. H. Madsen, D. S. Margulies, H. S. Mayberg, K. McMahon, C. S. Monk, S. H. Mostofsky, B. J. Nagel, J. J. Pekar, S. J. Peltier, S. E. Petersen, V. Riedl, S. A. Rombouts, B. Rypma, B. L. Schlaggar, S. Schmidt, R. D. Seidler, G. J. Siegle, C. Sorg, G.-J. J. Teng, J. Veijola, A. Villringer, M. Walter, L. Wang, X.-C. C. Weng, S. Whitfield-Gabrieli, P. Williamson, C. Windischberger, Y.-F. F. Zang, H.-Y. Y. Zhang, F. X. Castellanos, and M. P. Milham, “Toward discovery science of

- human brain function.” *Proceedings of the National Academy of Sciences of the United States of America*, vol. 107, no. 10, pp. 4734–4739, Mar. 2010. [Online]. Available: <http://dx.doi.org/10.1073/pnas.0911855107>
- [35] J. A. Brown, J. D. Rudie, A. Bandrowski, J. D. Van Horn, and S. Y. Bookheimer, “The UCLA multimodal connectivity database: a web-based platform for brain connectivity matrix sharing and analysis.” *Frontiers in neuroinformatics*, vol. 6, 2012. [Online]. Available: <http://dx.doi.org/10.3389/fninf.2012.00028>
- [36] R. Casanova, C. T. Whitlow, B. Wagner, M. A. Espeland, and J. A. Maldjian, “Combining graph and machine learning methods to analyze differences in functional connectivity across sex.” *The open neuroimaging journal*, vol. 6, pp. 1–9, 2012. [Online]. Available: <http://dx.doi.org/10.2174/1874440001206010001>
- [37] M. S. Çetin, F. Christensen, C. C. Abbott, J. M. Stephen, A. R. Mayer, J. M. Cañive, J. R. Bustillo, G. D. Pearlson, and V. D. Calhoun, “Thalamus and posterior temporal lobe show greater inter-network connectivity at rest and across sensory paradigms in schizophrenia.” *NeuroImage*, vol. 97, pp. 117–126, Aug. 2014. [Online]. Available: <http://view.ncbi.nlm.nih.gov/pubmed/24736181>
- [38] M. Andric and U. Hasson, “Global features of functional brain networks change with contextual disorder,” *NeuroImage*, vol. 117, pp. 103–113, Aug. 2015. [Online]. Available: <http://dx.doi.org/10.1016/j.neuroimage.2015.05.025>
- [39] F. Pedregosa, G. Varoquaux, A. Gramfort, V. Michel, B. Thirion, O. Grisel, M. Blondel, P. Prettenhofer, R. Weiss, V. Dubourg, J. Vanderplas, A. Passos, D. Cournapeau, M. Brucher, M. Perrot, and E. Duchesnay, “Scikit-learn: Machine Learning in Python,” *Journal of Machine Learning Research*, 2011. [Online]. Available: <http://www.jmlr.org/papers/volume12/pedregosa11a/pedregosa11a.pdf>

Table 1: Results of experiments on all fMRI datasets. Name/Location and size ( $n$ ,  $m$ ) are reported in the first three columns. Across two graph embeddings (DCE, DRE) and two graph kernels (WL, SP), the median  $acc_{cv}$  and the related  $p$ -value are reported for CBT, while just the  $p$ -value for KTST. In bold the cases of disagreement in the  $p$ -value of CBT vs. KTST, assuming a standard threshold for significance  $\theta = 0.05$ .

Dataset	DCE		DRE		WL kernel		SP kernel	
	$m$	$n$	CBT-SVM $acc_{cv}$	KTST $p$ -val	CBT-SVM $acc_{cv}$	KTST $p$ -val	CBT-SVM $acc_{cv}$	KTST $p$ -val
Beijing	109	65	0.655	0.000	0.637	0.000	0.590	0.018
Berlin	13	13	0.767	0.008	0.767	<b>0.054</b>	0.433	0.692
Cambridge	123	75	0.660	0.000	0.647	0.000	0.513	0.274
Cleveland	20	11	0.500	0.112	0.500	0.435	0.550	0.166
Dallas	12	12	0.483	0.537	0.417	0.735	0.600	0.191
ICBM	29	22	0.538	0.172	0.518	0.142	0.466	0.688
Leipzig	21	16	0.617	0.041	0.611	<b>0.056</b>	0.458	0.709
Milwaukee	31	15	0.500	0.057	0.519	<b>0.037</b>	0.546	0.164
NewYork	43	36	0.569	0.085	0.532	0.171	0.538	0.214
Oulu	66	37	0.654	0.000	0.607	<b>0.148</b>	0.526	0.214
Oxford	10	12	0.700	0.019	0.650	0.105	0.467	0.562
Saint Louis	17	14	0.479	0.581	0.500	0.938	0.450	0.712
Schizophrenia	46	40	0.647	0.010	0.641	0.008	0.591	<b>0.076</b>
Context.Disord.	19	19	-	-	-	-	0.757	0.002
								0.010
								0.558
								<b>0.192</b>
								0.068
								<b>0.003</b>
								0.911
								<b>0.711</b>
								0.336
								0.096
								0.580
								<b>0.204</b>
								0.657
								0.116
								0.332
								0.198
								0.450
								0.347
								0.498
								<b>0.029</b>
								0.063
								0.171
								0.517
								0.171
								0.578

Table 2: Results of the simulation. The frequency of Type I and Type II error (lower is better) of CBT and KTST across different effect sizes ( $\delta$ ) are reported, for different  $p$ -value thresholds ( $\theta = 0.05$  and  $\theta = 0.01$ ). In bold are indicated the cases in which KTST strongly differ w.r.t. CBT.

Ground Truth	$m$	$n$	$p(\text{Type I})$						$p(\text{Type II})$						
			$\theta = 0.05$			$\theta = 0.01$			$\theta = 0.05$			$\theta = 0.01$			
			CBT-SVMs	KTST	CBT-SVMs	KTST	CBT-SVMs	KTST	CBT-SVMs	KTST	CBT-SVMs	KTST	CBT-SVMs	KTST	
$H_0$ true ( $\delta = 0$ )	20	20	0.077	0.053	0.028	0.009	-	-	-	-	-	-	-	-	-
$H_0$ false ( $\delta = 0.25$ )	20	20	-	-	-	-	0.813	0.781	0.813	0.781	0.907	0.919	0.907	0.919	0.919
$H_0$ false ( $\delta = 0.5$ )	20	20	-	-	-	-	0.433	<b>0.264</b>	0.433	<b>0.264</b>	0.693	<b>0.498</b>	0.693	<b>0.498</b>	<b>0.498</b>
$H_0$ false ( $\delta = 0.75$ )	20	20	-	-	-	-	0.093	<b>0.020</b>	0.093	<b>0.020</b>	0.215	<b>0.070</b>	0.215	<b>0.070</b>	<b>0.070</b>
$H_0$ false ( $\delta = 1.0$ )	20	20	-	-	-	-	0.013	0.000	0.013	0.000	0.018	0.001	0.018	0.001	0.001